Nonlinear Dyn (2019) 96:2069–2085
https://doi.org/10.1007/s11071-019-04906-w

ORIGINAL PAPER

Multi-parameter-adjusting stochastic resonance in a standard tri-stable system and its application in incipient fault diagnosis

Z. H. Lai · J. S. Liu · H. T. Zhang · C. L. Zhang · J. W. Zhang · D. Z. Duan

Received: 22 August 2018 / Accepted: 20 March 2019 / Published online: 4 April 2019

Abstract The weak-signal detection approaches based on stochastic resonance (SR) are beneficial in detecting weak vibration signals from strong background noise. Therefore, many SR-based methods for mechanical incipient fault diagnosis appear. Among various nonlinear SR models, the underdamped tri-stable SR system, which has better output performance than other ones, has shown its potential superiority in weak-signal detection. The shortcomings for this model include its nonstandard forms of nonlinear potential functions and its inadequate research on parameter-adjusting mechanism for parameter-fixed noisy signals. In order to solve these issues, a standard tri-stable SR system is introduced in this paper and its SR performance is studied. Furthermore, a multi-parameter-adjusting SR (MPASR) model for the standard tri-stable system is proposed and its parameter adjustment rules for different input signals to produce SR are fully studied. At last, we propose a weak-signal detection method based on MPASR of the standard tri-stable system and employ two practical examples to demonstrate its feasibility in incipient fault diagnosis.

Keywords Nonlinear tri-stable system · Multi-parameter-adjusting stochastic resonance · Weak-signal detection · Incipient fault diagnosis

1 Introduction

Rotating machinery is one of the most commonly used parts in various machines such as compressors, centrifugal pump, motorized spindles and water turbines. A failure in rotating machinery may result in the breakdown of the entire machine, even a disastrous accident. Therefore, it is of great importance to monitor the operating condition of the rotating machinery and diagnose existent faults as soon as possible, thus avoiding the potential accidents through timely maintenance.

In the past few decades, many diagnosis technologies based on vibration, acoustics, temperature and liquid have been proposed for the health monitoring and fault diagnosis of the rotating machinery. Among all these diagnosis technologies, the vibration analysis technology is mostly used due to the rich con-

Z. H. Lai (✉)
College of Mechatronics and Control Engineering, Shenzhen University, Shenzhen 518060, People's Republic of China
e-mail: drlaizhihui@163.com

Z. H. Lai · J. S. Liu · H. T. Zhang · C. L. Zhang · J. W. Zhang
School of Mechatronics Engineering, Nanchang University, Nanchang 330031, People's Republic of China

Z. H. Lai
Key Laboratory of Lightweight and High Strength Structural Materials of Jiangxi Province, Nanchang University, Nanchang 330031, People's Republic of China

D. Z. Duan (✉)
State Key Laboratory of Mechanical Manufacturing Systems Engineering, Xi'an Jiaotong University, Xi'an 710049, People's Republic of China
e-mail: dzduan@163.com

dition information in vibration signals. However, the vibration-based analysis methods show limited detection performance when the fault signals are weak or even submerged in strong background noise. These conditions can be commonly found in the vibration signals with an early fault or from tough working environments. Therefore, the weak-signal detection technology under strong noise background plays an important role in the incipient fault diagnosis of rotating machinery to guarantee the accuracy of diagnosis.

In order to extract the weak fault features from noisy signals, various weak-signal detection approaches, such as wavelet transform [1], chaos theory [2] and empirical mode decomposition [3], have been studied recently and successfully applied in the incipient fault identification of rotating machinery. These methods can be classified as noise cancelation-based methods, which highlight the fault features through suppressing or canceling the noise embedded in vibration signals. Due to their intrinsic properties, these methods inevitably damage the incipient fault features in the de-noising process, thereby limiting their detection performance in the severe conditions where the incipient fault features are submerged in heavy noise background. Compared with these noise cancelation-based methods, a nonlinear phenomenon called stochastic resonance (SR) leads a type of noise utilization-based methods, which have intrinsic superiority in weak-signal detection by taking advantage of the noise to enhance the weak signals through some nonlinear systems.

SR describes a type of interesting nonlinear phenomena, in which the curve of signal-to-noise ratio (SNR) against noise intensity presents a single-humped shape with the help of nonlinear systems. The SR phenomena describe an optimal synergistic action of the input signal, noise and nonlinear systems and make it possible for the weak signals to strengthen their intensities by absorbing a certain fraction of the noise energy, thus highlighting the weak signals. SR was first proposed by Benzi to explain the switching of the Earth's climate between ice ages and periods of relative warmth over a roughly 100,000-year cycle [4]. Subsequently, SR phenomena have been successfully observed in several physical experiments [5,6]. Since then, this nonlinear phenomenon has received much attention from the physics and engineering community in the research areas such as dynamical nonlinearity [7,8], energy harvesting [9–11] and weak-signal detection, which has been successfully applied in incipient fault diagnosis for rotating machines through various specific SR-based detection approaches [12].

The performance of a SR-based weak-signal detection method is mainly determined by the form of its nonlinear system. In the past decades, many different SR systems and their nonlinear behaviors have been studied. All these nonlinear systems can be generally divided into overdamped systems and underdamped systems [13]. The former ones are described by first-order nonlinear equations such as the traditional Lanvegin equation [14,15], in which the momentum term of the dynamic system is neglected due to large damping, while the latter ones are described by second-order nonlinear equations such as the Duffing equation [16,17], in which the momentum term is reserved and the damping force is determined by the damping ratio. Research results show that the detection model based on underdamped systems has good adaptability to signals with different noise intensities due to the tunable damping ratio [18]. This is a great superiority in parameter-adjusted SR and its further application in weak-signal detection. Therefore, the underdamped systems are mostly used as weak-signal detection models.

Furthermore, the weak-signal detection performance in both overdamped and underdamped SR systems is also affected by the potential functions of the detection models. Research has shown that SR can appear in mono-stable systems [19,20]. However, most research on SR-based weak-signal detection focuses on the bi-stable systems [21,22] because the detection performance in a bi-stable model is better than that in a mono-stable system, and SR can be easily achieved in a bi-stable model by adjusting its system parameters. In recent years, SR in tri-stable systems has been studied as well. It is found that due to the accessible larger moving distance of Brownian particle in a tri-stable potential field, the output SR performance in a tri-stable system can be better than that in a mono-stable or a bi-stable system [23,24]. This provides a new solution to further enhance the SR-based weak-signal detection performance.

Therefore, SR in tri-stable systems and its application in weak-signal detection have attracted much attention from academic community. In theoretical research, Arathi et al studied the SR in a triple-well system and revealed the impact of the depth of the wells on the SR

performance [25]. Zhang et al considered the logical SR phenomenon in triple-well potential systems driven by Gaussian colored noise and found that the system can yield all logic behaviors without changing the characteristics of the systems [26,27]. Shi et al investigated the SR in a multi-stable system driven by Gaussian white noise; in his work, the expression of the output SNR is derived [28]. He also studied the stable state properties and mean first-passage time of a tri-stable system driven by non-correlated additive and multiplicative non-Gaussian noise and obtained the expressions of the stable state probability density function and mean first-passage time of the system [29]. Further, incipient fault diagnosis has been achieved by using tri-stable SR systems. Li et al proposed a multi-stable SR system which can be transferred between mono-stable model, bi-stable system and tri-stable model according to different system parameters and found that the tri-stable system not only increases the output SNR and improves the detection effect of SR, but also achieves the detection of low SNR signals and enhances the detection capability of SR for weak signals to some extent [24]. The proposed multi-stable SR system has been further utilized in mechanical fault diagnosis for rolling bearing faults [23] and gearbox faults [23,24]. Based on this multi-stable SR system, Shi et al further studied the signal feature extraction based on cascaded multi-stable SR de-noising and EMD method [30]. Moreover, Lu et al reported a tri-stable cantilever that exploits SR phenomenon for a study of signal amplification and filtering [31]; this system has been successfully used in periodic fault signal enhancement in rotating machine vibrations [32].

However, the expressions of tri-stable potential functions are not uniform at its early study stage. In the aforementioned papers, at least six different tri-stable potential functions are proposed to establish a SR system. In these potential functions, some of them cannot cover all possible tri-stable systems [13]; some of them can be transferred between mono-stable, bi-stable and tri-stable system depending on the selection of system parameters [23,24]; thereby, the best output performance cannot be always realized; some of them are derived from a real cantilever model [31,32]; hence, the adjustments for the system parameters are not convenient.

In order to solve the above-mentioned issues, a standard symmetrical tri-stable function, which can cover all possible tri-stable functions by adjusting the system parameters, was constructed using equilibrium parameters, and a standard underdamped tri-stable system driven by weak periodic signal and noise simultaneously was further proposed in [33]. It was found that this underdamped system can guarantee its tri-stable state no matter what the system parameters are, and it can cover all possible tri-stable systems; hence, it is superior to previous tri-stable SR systems. Therefore, this tri-stable SR system has great potential in weak-signal detection and incipient fault diagnosis. However, these applications have not been studied yet. In this paper, aiming at the parameter-fixed noisy signal, we attempt to utilize the standard underdamped tri-stable SR system to extract weak-signal features combing the parameter-adjusting method and realize incipient fault diagnosis for rotating machinery.

The remainder of this paper is organized as follows. In Sect. 2, we introduce the standard underdamped tri-stable system and its basic properties related to SR. In Sect. 3, the multi-parameter-adjusting SR (MPASR) in the standard tri-stable system is proposed, involving the model, parameter adjustment rules and simulation verification. Section 4 presents the procedure of the weak-signal detection based on MPASR of the standard tri-stable system, along with two practical examples of incipient fault diagnosis. Conclusion and summary are drawn in Sect. 5.

2 Standard tri-stable SR system

2.1 Introduction of a standard tri-stable system

A typical SR system, which consists of a nonlinear system, a weak signal and a source of noise, can be written as:

$$\ddot{x} + k\dot{x} + \frac{\mathrm{d}U(x)}{\mathrm{d}x} = s(t) + n(t) \tag{1}$$

In this system, k denotes the damping ratio; $U(x)$ describes a x-dependent potential function of the outer potential field; $s(t) = A\sin(2\pi f_0 t + \varphi)$ denotes a harmonic characteristic signal with amplitude A, frequency f_0 and initial phase φ; $n(t) = \sqrt{2D}\xi(t)$ is the noise, where $\xi(t)$ represents a source of Gaussian white noise with zero mean and unit variance and D is the noise intensity; $sn(t) = s(t)+n(t)$ denotes the system input signal; and $x(t)$ represents the system output signal.

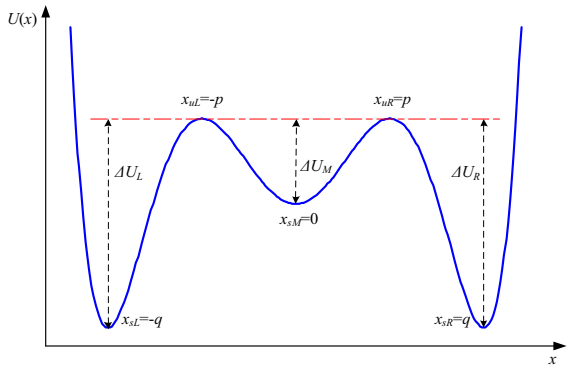

Fig. 1 Tri-stable potential field described by a standard tri-stable potential function

In Ref. [33], a standard tri-stable potential function is proposed:

$$U(x) = \frac{1}{2}ax^2 - \frac{1}{4}bx^4 + \frac{1}{6}cx^6 = \frac{m}{2}p^2q^2x^2 - \frac{m}{4}(p^2+q^2)x^4 + \frac{m}{6}x^6 \quad (2)$$

Here, $a = mp^2q^2$, $b = m(p^2+q^2)$ and $c = m$, where m, p and q $(p < q)$ are positive real numbers. Thus, Eq. (2) describes a symmetrical tri-stable potential field which contains three stable equilibrium points ($x_{sL} = -q$, $x_{sM} = 0$ and $x_{sR} = q$) and two unstable equilibrium points ($x_{uL} = -p$ and $x_{uR} = p$), as shown in Fig. 1. It can be seen that the potential filed is divided into three potential wells with depths equaling to ΔU_L, ΔU_M and ΔU_R, respectively. $\Delta U_{L,M,R}$ can be also regarded as the heights of the barriers between potential wells. Thus, Eq. (2) guarantees the potential field's tri-stable state. By adjusting the values of m, p and q, all possible tri-stable potential functions can be achieved.

The potential field strengths at five equilibrium points can be easily calculated through Eq. (2). It should be noted that $\Delta U_M = \Delta U_{L,R}$ when $q = \sqrt{3}p$, i.e., the middle and side potential wells have a same height. While when $q < \sqrt{3}p$, the middle potential well is deeper than the side ones ($\Delta U_M > \Delta U_{L,R}$); when $q > \sqrt{3}p$, the side potential wells are deeper than the middle one ($\Delta U_M < \Delta U_{L,R}$) [33].

For further qualitative analysis, the monotonicity conditions of ΔU_M and $\Delta U_{L,R}$ against parameters m, p and q are summarized in Table 1 [33].

By substituting Eq. (2) in Eq. (1), the latter equation can be rewritten as:

$$\ddot{x} + k\dot{x} + ax - bx^3 + cx^5 = A\sin(2\pi f_0 t + \varphi) + \sqrt{2D}\xi(t) \quad (3)$$

Thus, Eq. (3) describes a standard tri-stable system, and $x(t)$ can be considered as the position function of a Brownian particle moving in the presented potential field (see Fig. 1) under the input driving force $s(t)$ and noise $n(t)$.

2.2 SR in a standard tri-stable system

With respect to the standard tri-stable system described by Eq. (3), its output SNR [28], stable state probability density function (PDF) and mean first-passage time (MFPT) [29] were derived. It was found that SR can occur in such a tri-stable system [34]. The SR mechanism was also explained in terms of the steady-state solution curve [33]. It was reported that the noise metastatic capacity of a tri-stable SR system is better than the bi-stable SR system [23,24]. For this phenomenon, a visual explanation can be given with regard to the structure of the resonance models. For example, in the presence of the same input signal and noise, the moving distance of the Brownian particle in the tri-stable model in one cycle is greater than that in the classical bi-stable model when the resonance state is achieved; thus, the amplification effect of the former model on the weak signal is more obvious. A physical explanation can be also given that the tri-stable device system combines the benefits of bi-stable system (wide interwell spacing) and mono-stable system (smooth motion in potential) [31]. This superiority of tri-stable SR than bi-stable SR was also demonstrated through numerical calculations based on an optimization algorithm [35]. Therefore, the SR in a tri-stable has potential advantages in weak-signal detection and further fault diagnosis.

A special case is presented in this subsection to present the output performance of the standard tri-stable system. In Eq. (3), the parameters are set as $k = 0.5, m = 1, p = 0.5, q = 1.2, A = 0.1$, $f_0 = 0.01$ Hz, $\varphi = 0$, and the values of D vary from 0 to 1. The sampling frequency of the input signal is $f_s = 5$ Hz, and the number of calculating points $N = 20{,}000$. The fourth-order Runge–Kutta algorithm is adopted in this paper to solve Eq. (3) and obtain the system output.

Table 1 Monotonicity conditions of ΔU_M and $\Delta U_{L,R}$ against m, p and q

	$m(m > 0)$	$p(0 < p < q)$	$q(q > p)$
ΔU_M	Monotonically increasing	Monotonically increasing	Monotonically increasing
$\Delta U_{L,R}$	Monotonically increasing	Monotonically decreasing	Monotonically increasing

Define $\mathrm{Am_{in}}$ and $\mathrm{Am_{out}}$ as the amplitude values corresponding to characteristic signal frequency at system input and output, respectively. Similarly, define $\mathrm{SNR_{in}}$ and $\mathrm{SNR_{out}}$ as the signal-to-noise ratios at system input and output, respectively:

$$\begin{cases} \mathrm{SNR_{in}} = 10\log_{10}\left(\frac{\mathrm{Am_{in}^2}}{\sum[SN(f)]^2-\mathrm{Am_{in}^2}}\right) \\ \mathrm{SNR_{out}} = 10\log_{10}\left(\frac{\mathrm{Am_{out}^2}}{\sum[X(f)]^2-\mathrm{Am_{out}^2}}\right) \end{cases} \tag{4}$$

Here, $SN(f)$ represents the single-side spectrum of system input $sn(t)$ and $X(f)$ the spectrum of system output $x(t)$. Thus, $\mathrm{Am_{in}} = SN(f_0)$ and $\mathrm{Am_{out}} = X(f_0)$. Apparently, the values of $\mathrm{Am_{in}}$ and $\mathrm{Am_{out}}$ indicate the absolute strength of the characteristic signal in system input and output, respectively, while the values of $\mathrm{SNR_{in}}$ and $\mathrm{SNR_{out}}$ indicate the ability of the signal to be identified. As the values of D vary from 0 to 1, the trends of $\mathrm{Am_{in}}$, $\mathrm{Am_{out}}$, $\mathrm{SNR_{in}}$ and $\mathrm{SNR_{out}}$ against D are plotted in Fig. 2.

It can be seen from Fig. 2 that as D increases, the characteristic signal amplitude ($\mathrm{Am_{in}}$) increases slightly, while the input SNR ($\mathrm{SNR_{in}}$) drops significantly. However, both $\mathrm{Am_{out}}$-D and $\mathrm{SNR_{out}}$-D curves generally present an increasing trend until an optimal noise intensity $D = D_{\mathrm{op}}$ (where SR occurs) and then a decreasing trend. This is a typical nonlinear SR performance, which indicates that the standard tri-stable system described by Eq. (3) can produce SR under a set of appropriate system parameters (k, m, p and q) and signal/noise parameters (A, f_0, φ and D). When SR occurs, the noise can help the Brownian particle to accumulate energy so that it can jump from one side potential well to another one regularly, thus resulting in a much larger motion displacement for the particle and producing a much larger characteristic signal amplitude at output than that at input. Moreover, the output SNR is much larger than the input SNR at SR, indicating that the weak characteristic signal is much easier to be detected in the output than in the input.

3 Multi-parameter-adjusting SR in the standard tri-stable system

It can be seen from Sect. 2.2 that SR presents a synergy between the signal, noise and nonlinear system. SR can only occur when the selections of signal, noise and system parameters are appropriate. For example, Fig. 2 shows that SR can only appear at optimal noise intensity D_{op} when other parameters are fixed. Similarly, when the signal and noise parameters are fixed, SR can only occur when the system parameters are appropriate. Under the fixed noisy signal, the SR achieved through adjusting system parameters is the so-called parameter-adjusting SR.

In the practical application of incipient fault diagnosis, the signal and noise parameters of the detected vibration signal are fixed. In order to extract the weak fault signal through the SR in the proposed standard tri-stable system, it is necessary to study its parameter-adjusting SR method, which will be introduced in this section.

3.1 MPASR model for the standard tri-stable system

The SR mechanism in the standard tri-stable system (3) has been studied in Ref. [33] from the aspect of system steady-state solution curve. It can be explained that SR can only occur when A, f_0 and D are all small parameters. Therefore, there are two significances in studying the parameter-adjusting SR in a standard tri-stable system. Firstly, it can overcome the rigorous small-parameter limitation for the system to produce SR. Secondly, the system can also produce SR by adjusting one or more adjustable parameters when the signal, noise and system are unmatched.

In the standard tri-stable system Eq. (3), the test signal $sn(t)$ is mainly determined by the fixed parameters A, f_0, φ and D. In these signal parameters, φ has little influence on the system output. When A is too large or too small, we can simply transform the amplitude of the test signal by multiplying an

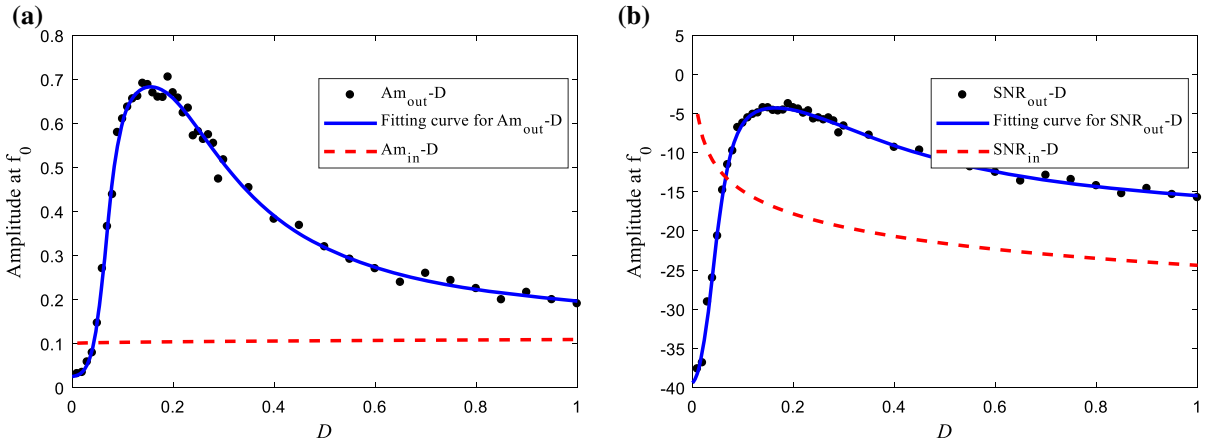

Fig. 2 **a** Am-D curves and **b** SNR-D curves of the standard tri-stable system

amplitude-transformation coefficient. Considering that f_0 is always a large parameter in engineering vibration signals, the test signals' time/frequency scale should be numerically compressed by simply using $\Delta t' = R/f_s$ as the time step instead of $\Delta t = 1/f_s$ in numerical calculations [36]. When the value of D is not appropriate, adjusting the system parameters k, m, p, q is helpful to realize SR. Combining all the mentioned parameter-adjusting method, a multi-parameter-adjusting SR (MPASR) model for the standard tri-stable system Eq. (3) to produce SR under fixed test signals can be written:

$$\begin{aligned}&\ddot{x}(t') + k\dot{x}(t') + ax(t') - bx(t')^3 + cx(t')^5 \\ &= \varepsilon\left[A\sin(2\pi f_0' t' + \varphi) + \sqrt{2D}\xi(t')\right] \\ &= \varepsilon A\sin(2\pi f_0' t' + \varphi) + \sqrt{2\varepsilon^2 D}\xi(t')\end{aligned} \tag{5}$$

Here, ε is an amplitude-transformation coefficient. $t' = Rt = R/f_s$ represents the timescale transformed by the scale-transformation coefficient R; this is realized by setting the time step as $\Delta t' = R/f_s$ instead of $\Delta t = 1/f_s$ in calculations; thus, the frequency of the input test signal becomes $f_0' = f_0/R$, and the system output in terms of scale t' can be obtained as $x(t')$. What should be pointed out is that both amplitude and scale transformation in numerical calculations are equivalent to corresponding system parameter adjustments in the model [36]. They do not change any characteristics of the given test signal $sn(t)$ and provide much simpler adjusting forms.

3.2 Parameter adjustment rules

In the MPASR model Eq. (5), ε and R are adjusted for unmatched A and f_0, respectively, and the rest parameters including k, m, p, q are adjusted for the unmatched input noise intensity $D' = \varepsilon^2 D$. The influence of the parameters k, m, p and q on the system output performance can be obtained in terms of the particle transition between two side wells in the tri-stable potential field.

Assuming that the side potential wells are deeper than the middle one, i.e., $q > \sqrt{3}p$, the SR in the standard tri-stable system can be regarded as the particle transition between two side potential wells in accordance with the change of the weak periodic force $(s(t))$. Under the premise that the energy of input characteristic signal is not large enough for the particle to jump between potential wells, the transition ability for the particle is determined by the noise, the inhibition from the system and the shape of potential field.

Firstly, the value of noise intensity D is positively related to the particle's transition ability. When D is large, the particle can easily accumulate energy to jump from one side potential well to another one. It should be pointed out that we ignore the middle potential well because it is shallower than the side ones and the particle can jump out from it definitely; while when D is small, the particle can hardly jump out from either side potential well due to inadequate energy.

Secondly, the value of damping ratio k is negatively related to the particle's transition ability. The term of $k\dot{x}$ in Eq. (5) indicates the inhibition for the particle's

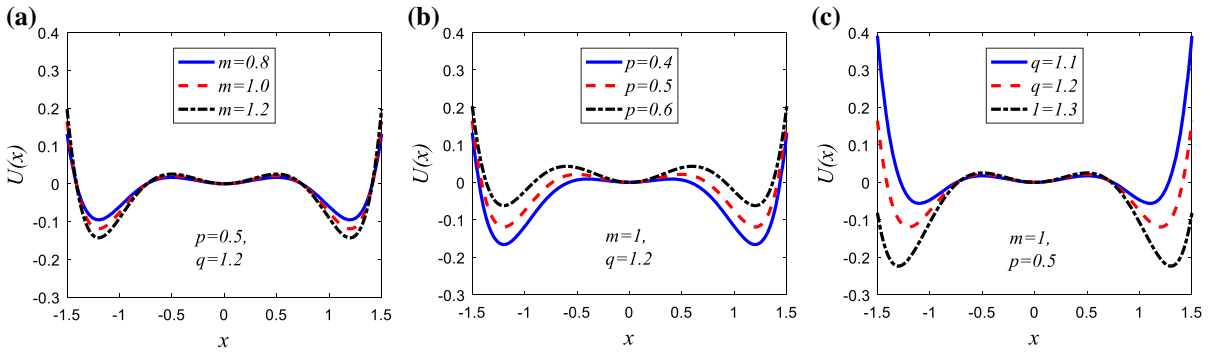

Fig. 3 Influences of **a** m, **b** p and **c** q on the shapes of the tri-stable potential fields

motion from the medium in the potential field. It is easy to understand that when k is smaller, the particle can jump out from one side potential well easier due to the smaller inhibition force, and vice versa. It can be seen that k has an opposite effect on the particle's transition ability comparing to D. Therefore, we can seek an optimal k to match different D, thus producing SR in Eq. (5) with the particle's transition ability kept at an appropriate level.

Last, the shape of the potential field also affects the particle's transition ability: The more deeper and steeper of the side potential well, the harder for the particle to jump out, and vice versa. It can be seen from Table 1 that under the premise of $q > \sqrt{3}p$, the side potential wells will be deeper with a larger m, q or a smaller p, which can be also seen from Fig. 3. This is to say, m and q have a negative influence for the particle's transition ability, and p has positive influence. Therefore, when D is too small, we can decrease the values of m and q or increase the value of p to help the particle to jump out easier; while when D is too large, we can increase the values of m and q or decrease the value of p.

The $\mathrm{Am_{out}}$-D curves for different system parameters are presented in Fig. 4. It can be seen that the optimal noise intensity D_{op} has a positive correlation with k, m and q and a negative correlation with p. These rules accord with the previous analyses. Moreover, the values of $\mathrm{Am_{out}}$ at SR points remain at a stable level as the value of k changes (see Fig. 4a) due to the same level of particle's transition ability at each case, while they significantly drop as the values of m, q become larger (see Fig. 4b, d) and that of p becomes smaller (see Fig. 4c). Therefore, in order to realize the MPASR in Eq. (5) under unmatched D, k should be set as the main adjusting parameter. On the other hand, m, p and q can be set as minor adjusting parameters. When the system output is under-resonant (i.e., the input noise intensity D is too small), we can decrease the value of k to achieve SR and decrease the values of m, q or increase that of p slightly to achieve a better SR output. While when the system output is over-resonant (i.e., the input noise intensity D is too large), we should increase the value of k and do not adjust m, p and q due to their negative influences on the SR output performance.

According to above analyses, the parameter adjustment rules for the standard tri-stable system Eq. (5) to produce SR under unmatched signal amplitude A, frequency f_0 (being too large in most cases) and noise intensity D are summarized in Table 2. It can be seen that the parameter adjustment rules for A and f_0 are simple and unique. However, there exist several optional adjustment methods for D, especially when it is too small.

3.3 Simulation verification

In order to verify the adjustment rules and detection performance of the proposed MPASR method based on standard tri-stable system for low SNR signals, a simulated noisy signal is generated and then processed in this subsection.

The test signal $sn(t) = s(t) + n(t)$ is generated with $A = 0.01$, $f_0 = 10$ Hz, $\varphi = 0$, $D = 0.02$. The sampling frequency of the test signal is $f_s = 5000$ Hz and the number of calculating points $N = 4096$. The waveform and spectrum of the generated test signal are shown in Fig. 5a, b. It can be seen that due to the

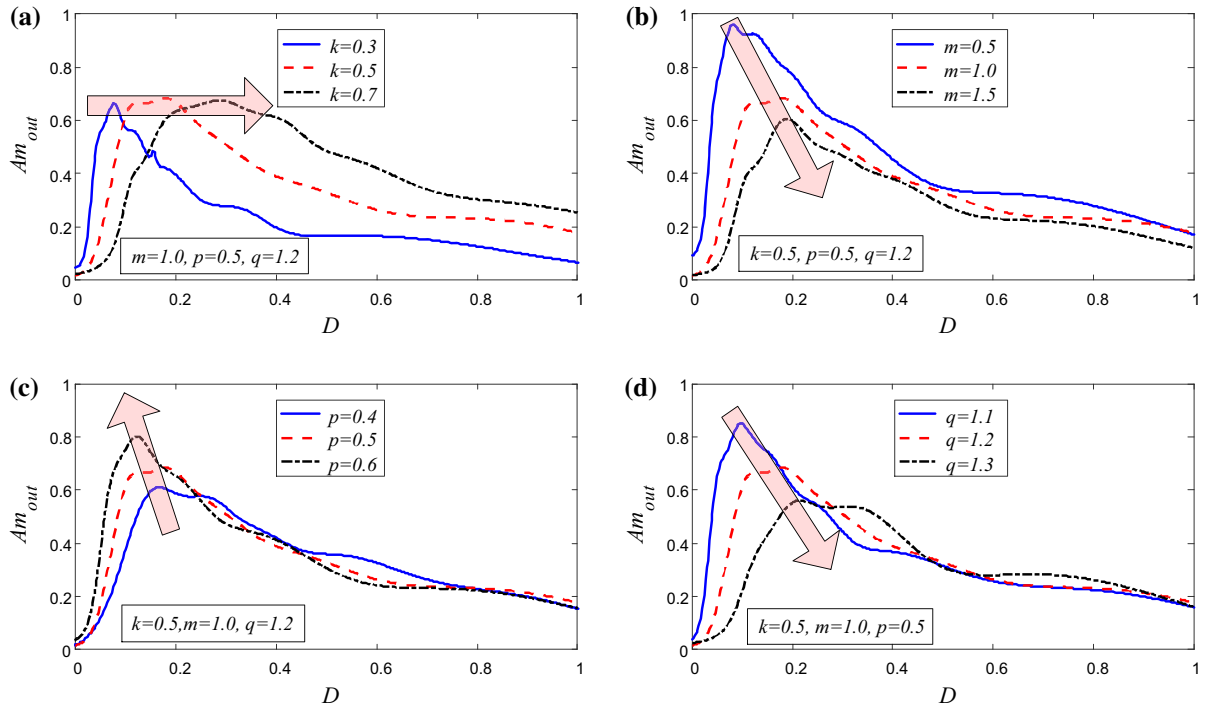

Fig. 4 Output signal amplitude $\mathrm{Am_{out}}$ as a function of different **a** k, **b** m, **c** p and **d** q

Table 2 Parameter adjustment rules for SR in the standard tri-stable system under unmatched signal amplitude A, frequency f_0 (being large parameter) and noise intensity D

A		f_0	D	
Too small	Too large	Too large	Too small (under-resonant)	Too large (over-resonant)
Increase ε	Decrease ε	Increase R	Mainly decrease k. Slightly decrease m, q, or increase $p(q > \sqrt{3}p)$	Increase k

strong background noise ($\mathrm{SNR_{in}} = -27.95$ dB), the weak signal cannot be identified in either waveform or spectrum. In order to confirm the existence of the weak signal and extract its characteristic parameters such as frequency, the MPASR method based on the standard tri-stable is adopted to process the test signal.

In Eq. (5), the system parameters are preliminarily set as $\varepsilon = 1$, $R = 1$, $k = 0.5$, $m = 1$, $p = 0.5$ and $q = 1.2$. The system output can be obtained with the test signal being input, as shown in Fig. 5c, d. As the signal frequency $f_0 = 10$ Hz greatly exceeds the small-parameter limitation of the SR in the tri-stable system, and the signal amplitude is too small, the system cannot produce SR and the weak signal also fails to be identified from the output waveform and spectrum. Therefore, the MPASR method should be further employed to analyze the test signal.

Firstly, the values of ε and R are adjusted to 10 and 1000, respectively. Hence, the amplitude and frequency of the input signal after transformation are $\varepsilon A = 0.1$ and $f_0/R = 0.01$ Hz, both of which satisfy the small-parameter limitation. The waveform and spectrum of the output signal are plotted in Fig. 5e, f, where the original time/frequency scale is used. It can be seen from Fig. 5e that the system output realizes the inter-well transitions. However, the noise intensity of the input signal after transformation becomes $\varepsilon^2 D = 2$, which is too large for the tri-stable system to produce SR. Therefore, the system is over-resonant. Again, the characteristic signal cannot be identified from the output signal.

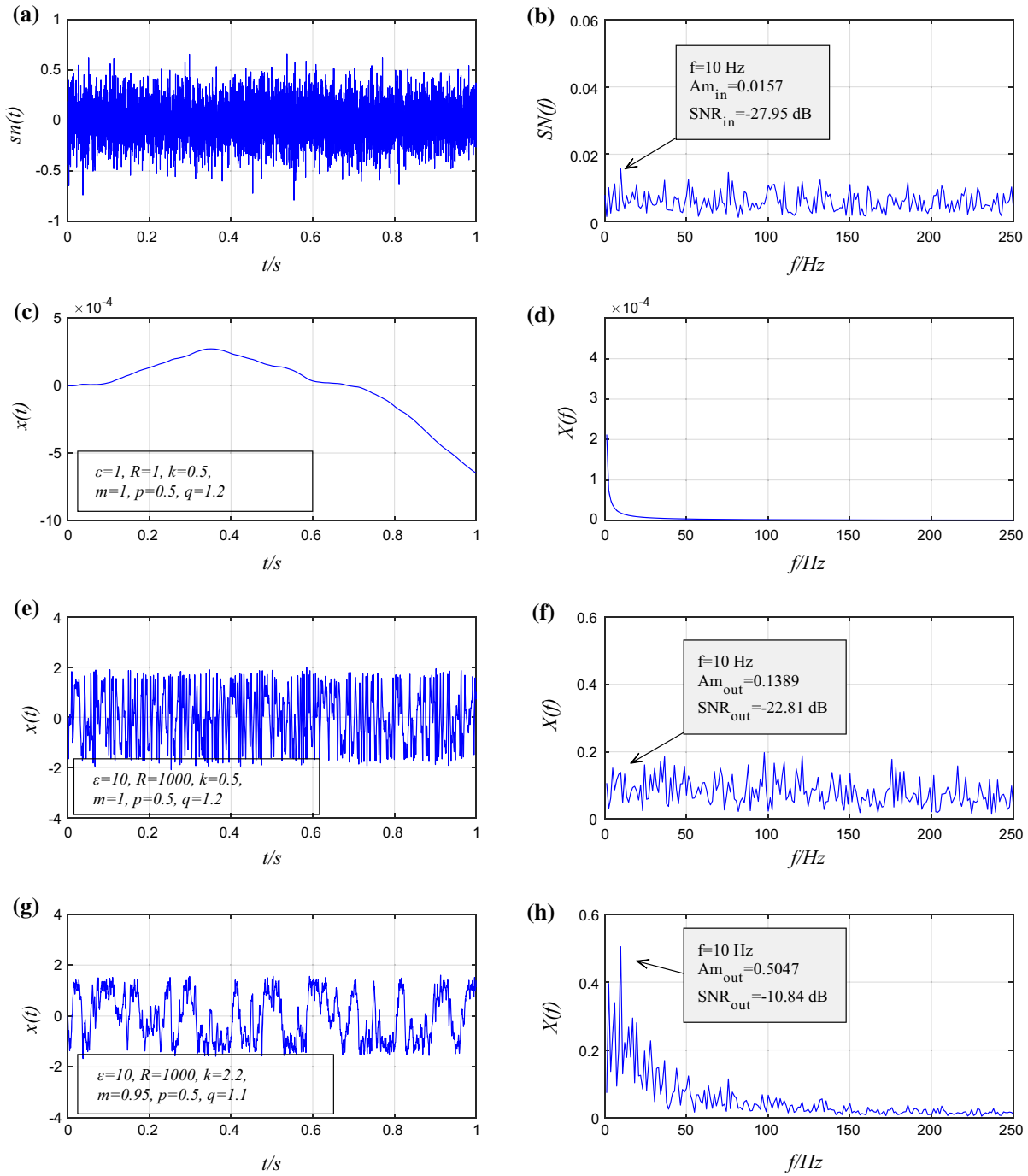

Fig. 5 Waveforms and spectrums of the input signal (**a**, **b**) and output signals (**c**–**h**) under different system parameters in the standard tri-stable MPASR system

Then, the value of k is increased to 2.2, and the values of m, p and q are adjusted slightly according to the output signal. Thus, all the signal parameters and system parameters are matched and SR appears in the tri-stable system, as shown in Fig. 5g, h. It can be seen in Fig. 5h that under the SR condition, the output SNR

($\mathrm{SNR_{out}} = -10.84$ dB) is greatly enhanced. Therefore, the characteristic signal with frequency $f_0 = 10$ Hz can be identified in the noisy input signal by using the standard tri-stable MPASR model.

4 Practical examples

4.1 Weak-signal detection method based on MPASR of the standard tri-stable system

The vibration signals $sn(t)$ of the rotating machinery with incipient faults are generally noisy signals. It is difficult to identify the characteristic fault signal in the test signal and diagnose the machines' incipient faults. Considering that a steady-state signal $sn(t)$ in practical engineering can be decomposed into some periodic signals and a source of noise, the standard tri-stable system can produce SR with $sn(t)$ being input under appropriate parameter conditions according to previous analyses. Thus, a weak-signal detection method based on the MPASR of the standard tri-stable system is proposed in this subsection to realize the incipient fault diagnosis of rotating machinery. The detection model can be written as:

$$\ddot{x}(t')+k\dot{x}(t')+ax(t')-bx(t')^3+cx(t')^5 = sn'(t') \quad (6)$$

The parameters in this model have the same meanings with Eq. (5). Here, $sn(t)$ represents the test vibration signal with incipient fault; ε is the amplitude-transformation coefficient, and t' is the transformed timescale corresponding to R; thus, $sn'(t') = \varepsilon sn(t')$ is the input signal of the detection model after an amplitude transformation and a scale transformation.

According to the parameter adjustments rules summarized in Table 2, the basic ideas for Eq. (6) to produce SR can be obtained. First we adjust the values of ε and R until the amplitude and frequency of the input signal $sn'(t')$ satisfy small-parameter limits, and then, adjust k, m, p and q to match with the noise intensity of $sn'(t')$. If SR appears in the proposed detection model under appropriate parameters, the weak fault signal can be identified and the fault diagnosis is realized. While if SR cannot appear through parameter adjustments, we can say no faults exist. The flowchart of the proposed method for incipient fault diagnosis is shown in Fig. 6, and two incipient fault diagnosis examples are presented to demonstrate the feasibility of the proposed weak-signal detection method in the next subsection.

4.2 Diagnosis of the shaft-bending fault in a sliding-bearing system

Shaft bending, referring to a situation where the axis of the shaft does not overlap with that of the rotation, is a common rotating machinery fault type, which results in vibrations in the unbalanced rotor and potential damage for the rotating machine. The vibration signal of the rotator has an obvious fundamental frequency, often accompanied by the second- or higher-order harmonics. This feature is helpful for us to diagnose the rotor shaft-bending fault in rotating machinery.

A shaft-bending fault experiment was performed on a sliding-bearing experimental table, where the shaft diameter was $\phi 12$ mm, as shown in Fig. 7. In the test, the deviation between the shaft axis and the rotation one is 0.38 mm, indicating a shaft-bending fault. An accelerometer was placed at the experimental table 0.5 m far from the bearing base, indicating a long distance of propagation path. During the test, the motor-driven rotor was rotated at an angular speed of 1680 rpm, i.e., a frequency of 28 Hz. Vibration signals with the shaft-bending fault were collected using a signal-acquiring device of type NI PXI-1033 (National Instrument Corporation, Austin, Texas, USA) at 5000 samples per second ($f_s = 5000$), and the data length is $N = 5000$.

The waveform, global spectrum and low-frequency spectrum (0–500 Hz) of the collected vibration signal are shown in Fig. 8. It can be seen from Fig. 8a that the fault signal was weak and nearly overwhelmed in the strong background noise. In the spectrums of Fig. 8b, c, although a signal component with frequency $f = 28.08$ Hz, which corresponds to the rotational frequency, can be observed, it was not prominent comparing to other signal components ($\mathrm{SNR_{in}} = -26.05$ dB). Therefore, we cannot say whether the vibration signal contains fault features.

In order to further analyze the vibration signal, the proposed weak-signal detection method is further employed. We input the collected vibration $sn(t)$ into Eq. (6) and chose [20 Hz, 35 Hz] as detecting frequency. Firstly, ε was set as 200, and R was set as 1000 to transform the detecting frequency domain into [0.02 Hz, 0.035 Hz] within an appropriate small-parameter

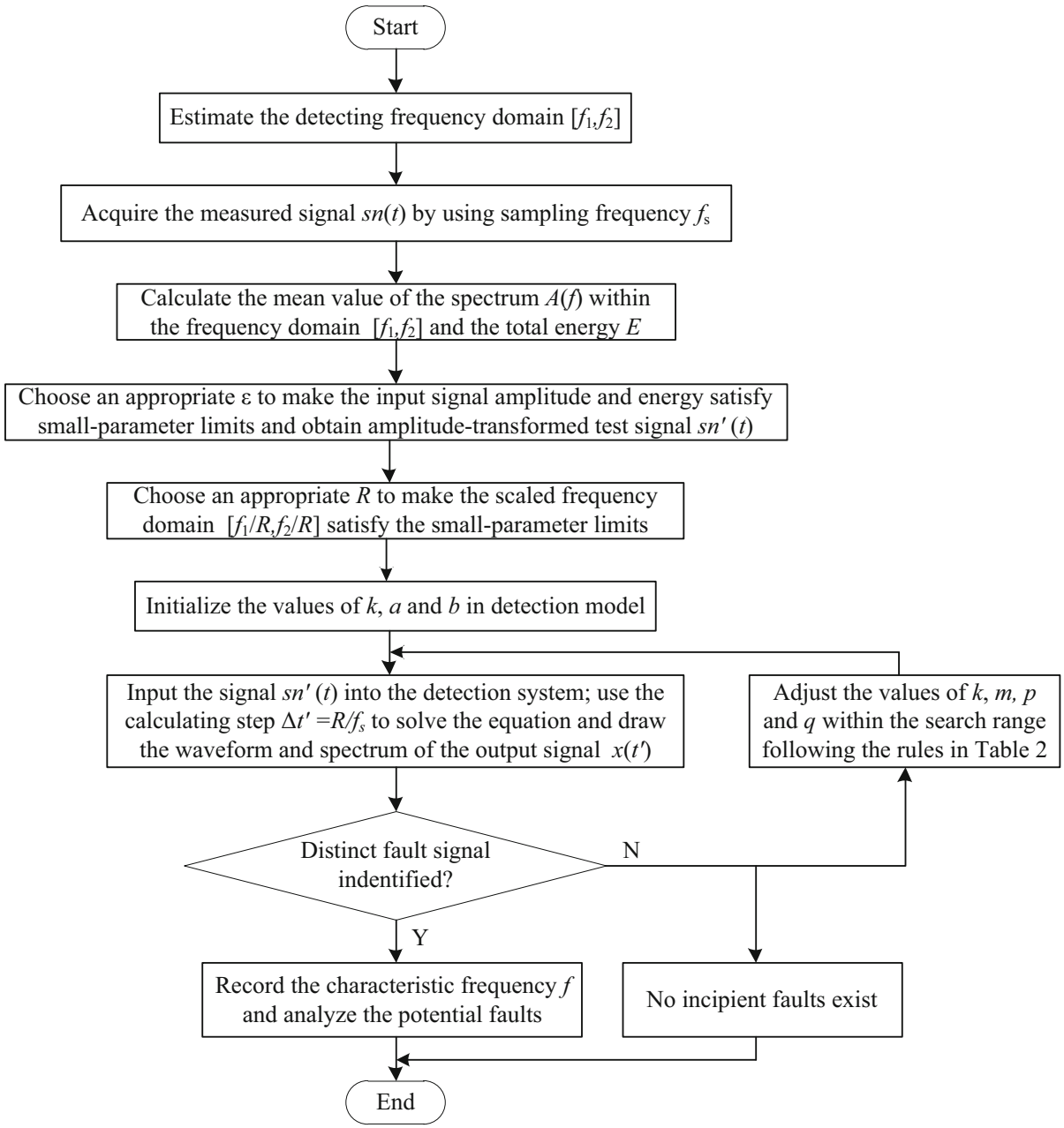

Fig. 6 The flowchart of the proposed incipient fault diagnosis method based on MPASR of the standard tri-stable systems

range; by adjusting other parameters in Eq. (6), a detection result was shown in Fig. 9 with $k = 5$, $m = 1.2$, $p = 0.6$ and $q = 1.3$ (the frequency parameter was scale transformed using the real sampling frequency). It can be seen that the output spectrum presents a signal component ($f = 28.08$ Hz, corresponding to the rotational frequency) with its amplitude much larger than others ($\mathrm{SNR_{out}} = -6.36$ dB). This result indicates that there must be a shaft-bending fault or a misalignment fault in the rotating system. The most distinct difference between these two faults is that obvious second- or higher-order harmonic components only exist in the vibration signal of the rotor with a shaft-bending fault. However, no higher-order harmonics can be observed

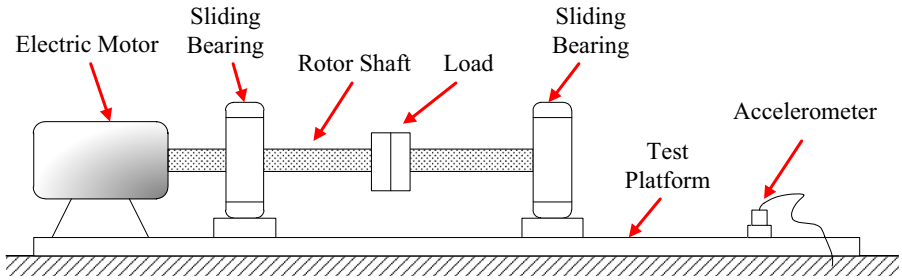

Fig. 7 Sliding-bearing experimental table for shaft-bending fault experiments

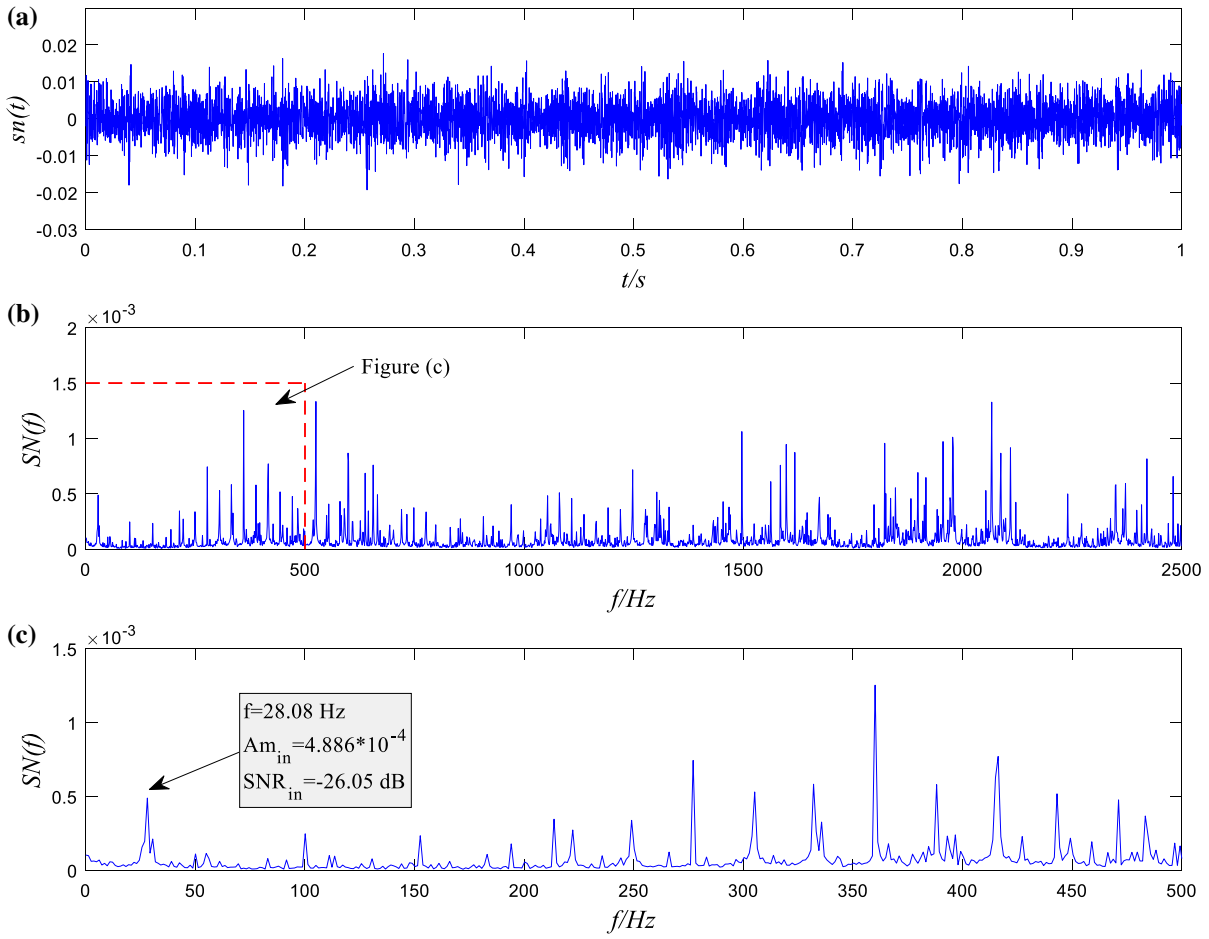

Fig. 8 Original vibration signal with shaft-bending fault. **a** Waveform; **b** global spectrum; **c** low-frequency spectrum

in Fig. 9. Therefore, we continued to adjust the parameters in the detection system Eq. (6) to further confirm what kind of fault the rotating system had.

Considering that the potential second- or higher-order frequencies were larger than the fundamental frequency, we should increase the value of R according to Table 2. We reset $R = 2000$ and the values of other parameters. When $k = 3$, $m = 1$, $p = 0.5$ and $q = 1.2$, another detection result is shown in Fig. 10, in which we could see obvious fundamental frequency component and also the second- and higher-order harmonics. Therefore, we were able to diagnose that a shaft-bending fault exists in the rotating system, which was accordant with the real physical truth of the system. Thus, the diagnosis of a shaft-bending fault was realized by using the weak-signal detection method

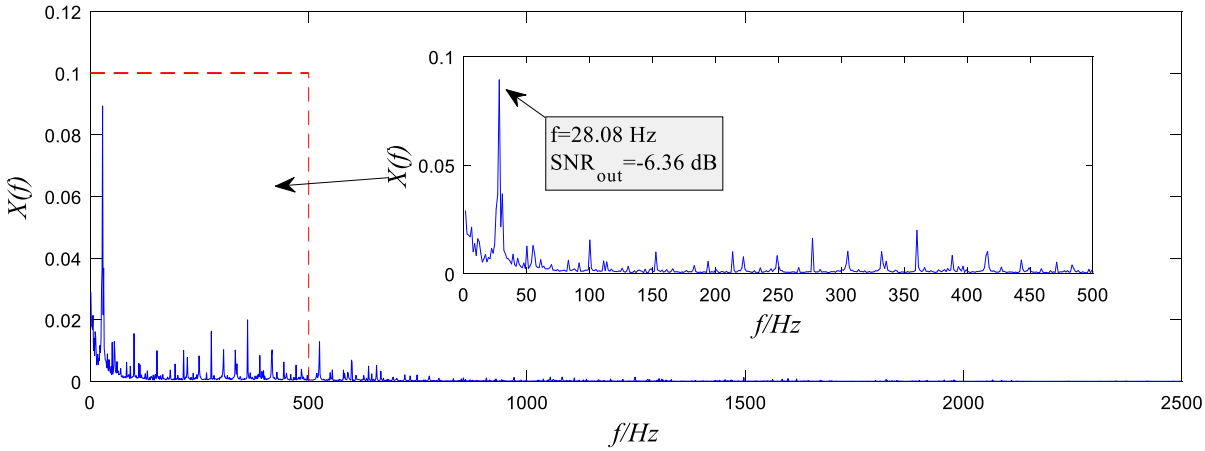

Fig. 9 The output global and low-frequency spectra of the standard tri-stable system with the vibration signal being input. The corresponding parameters in the detection system are set as $\varepsilon = 200$, $R = 1000$, $k = 5$, $m = 1.2$, $p = 0.6$ and $q = 1.3$

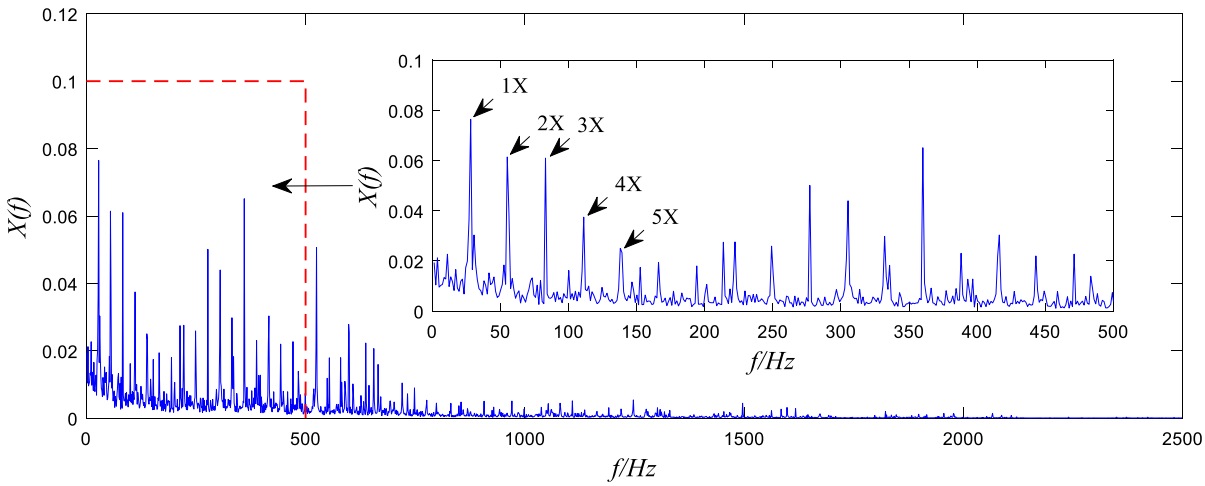

Fig. 10 The output global and low-frequency spectra of the standard tri-stable system with the vibration signal being input. The corresponding parameters in the detection system are set as $\varepsilon = 200$, $R = 2000$, $k = 3$, $m = 1$, $p = 0.5$ and $q = 1.2$

based on the MPASR in the standard tri-stable system.

The same fault signal shown in Fig. 8 has been processed previously by using the SR in a bi-stable Duffing system [18]. It can be seen that the output SNR in Fig. 9 (-6.36 dB) is much larger than that in Fig. 8 of Ref. [18] (-37.51 dB), and more higher-order harmonics can be identified in Fig. 10 than in Fig. 9 of Ref. [18]. This comparison result provides a strong support that the tri-stable SR system has better weak-signal detection performance than the bi-stable SR system in practical applications.

4.3 Diagnosis of a rolling bearing inner raceway fault (Case West Reserve data)

To further validate the applicability of the proposed weak-signal detection method, a vibration signal of rolling bearing with inner raceway fault is analyzed in this subsection. The bearing fault signal is cited from the Case Western Reserve University (CWRU) Bearing Data Center, which provides data presenting various degrees of difficulty for diagnosis [37]. The basic layout of the test rig is shown in Fig. 11. It consists of a 2-hp reliance electric motor driving a shaft on which a

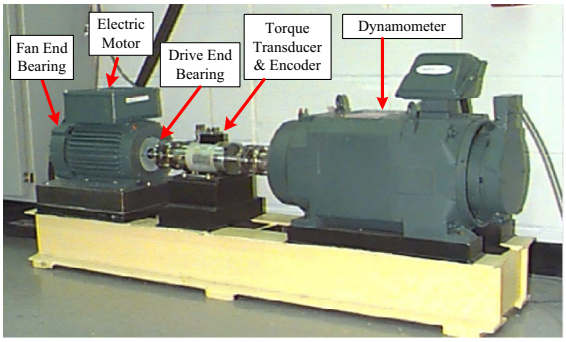

Fig. 11 CWRU bearing test rig

torque transducer and encoder are mounted. Torque is applied to the shaft via a dynamometer and electronic control system.

In the test, a fault of 0.021 inches in diameter was seeded on the inner raceway of the drive end bearing, which is a deep groove ball bearing with the type of SKF 6205-2RS JEM. The geometric parameters and fault frequencies of the bearing are provided in Table 3. A characteristic frequency f_{BPFI} and its high-order harmonics are expected components in the bearing's vibration spectrum when the fault appears in inner raceway. An accelerometer was placed at the 12 o'clock position at the drive end of the motor housing. During the test, the shaft speed was 1796 rpm ($f_0 = 29.93$ Hz), and thus, $f_{\mathrm{BPFI}} = 162.10$ Hz. Vibration signals were collected using a 16-channel DAT recorder at 48,000 samples per second ($f_s = 48{,}000$ Hz) for the drive end faults, and the data length is $N = 10{,}000$.

The waveform and spectrum of the collected vibration signal are shown in Fig. 12. It can be seen that due to the strong background noise, the signal component with fault frequency $f_{\mathrm{BPFI}} = 161.9$ Hz is quite weak with $\mathrm{SNR_{in}} = -41.24$ dB, and no higher-order harmonics can be observed. Therefore, the inner raceway fault of the bearing cannot be diagnosed in the original signal.

The proposed weak-signal detection method based on MPASR of the standard tri-stable system is further adopted to analyze the vibration fault signal. We input the collected vibration $sn(t)$ into Eq. (6), where $\varepsilon = 10$ and $R = 9600$ were selected to transform the amplitude and scale of the test signal. The first detection result is shown in Fig. 13a, where the fault characteristic frequency component is prominent ($\mathrm{SNR_{out}} = -25.43$). Another detection result is shown in Fig. 13b, in which the second- and higher-order harmonics are also obvious besides the fault characteristic frequency component. Thus, we were able to say that the bearing had an inner raceway fault. The diagnosis of a rolling bearing inner raceway fault was successfully realized by using the weak-signal detection method based on the MPASR in the standard tri-stable system.

4.4 Discussion

The feasibility of the proposed weak-signal detection method based on MPASR of the standard tri-stable system has been verified through two practical examples in this section. It can be seen that the weak fault features can be enhanced by properly adjusting the system parameters to produce SR in the standard tri-stable system.

What should be pointed out is that in order to better present the adjustment rules and performance of the proposed method, we used manual adjustments in this paper. It is apparent that the success of manual adjustments relies on the experience of the engineer. Therefore, it is inconvenient and inefficient in practical applications. Fortunately, the proposed method can be easily combined with multi-parameter optimization methods such as particle swarm optimization (PSO) algorithm. Thus, the adaptive parameter adjustments and further online detection based on the proposed method can be easily realized.

In this section, we only consider the cases of single fault to demonstrate the feasibility of the proposed weak-signal approach. In practical applications, the feature extraction from weak and coupled multi-faults signal is quite difficult. However, the detection results in this section show that we can extract weak signals of different frequencies by set different parameters, thus indicating the potential of the proposed method in the diagnosis of multi-faults. This is worthy of further study in the near future.

5 Conclusion and summary

In this paper, a standard underdamped tri-stable SR system has been proposed and studied. This model consists of a weak signal, a source of noise and a standard tri-stable system, which is constructed by using

Table 3 Bearing details and fault frequencies

Position on rig	Model number	Inside diameter (inches)	Thickness (inches)	Ball diameter (inches)	Pitch diameter (inches)	No. of rolling elements	Fault frequencies f_{BPFI} (multiple of shaft speed)
Drive end	SKF 6205-2RS JEM	0.9843	2.0472	0.5906	1.537	9	5.4152

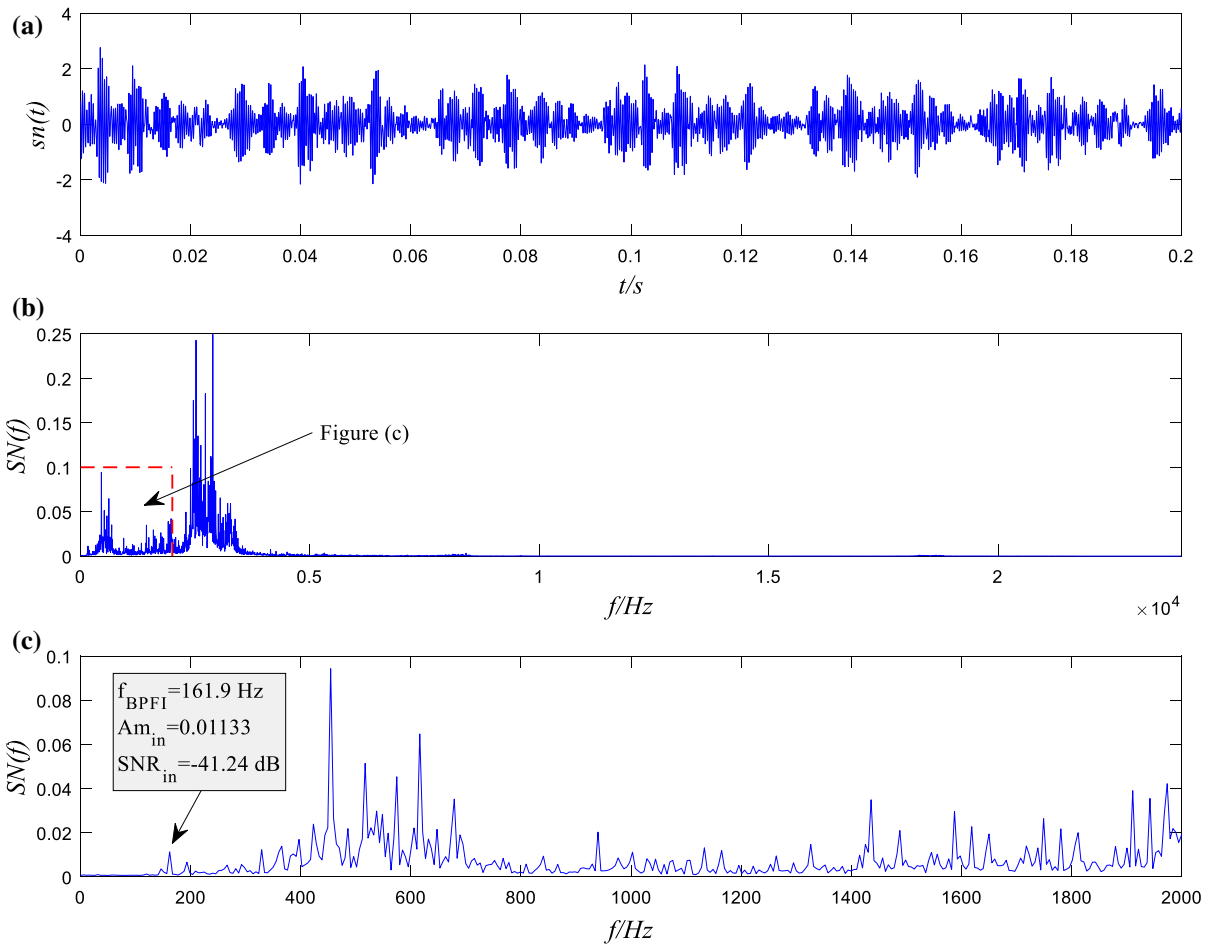

Fig. 12 Original vibration signal with bearing inner raceway fault. **a** Waveform; **b** global spectrum; **c** low-frequency spectrum

two equilibrium points and one unequilibrium point. SR can appear in this standard tri-stable system under appropriate parameter conditions, thus producing much larger signal-to-noise ratio (SNR) in the system output. In order to achieve SR in this system for different test vibration signals, whose signal and noise parameters are fixed, a multi-parameter-adjusting SR (MPASR) model is proposed for the standard tri-stable system, and its parameter adjustments rules are fully studied and summarized. Thus, the proposed MPASR model can achieve SR for fixed test signals by adjusting multi-parameters such as the damping ratio, amplitude-transformation coefficient, scale-transformation coefficient and the system parameters. Based on the MPASR

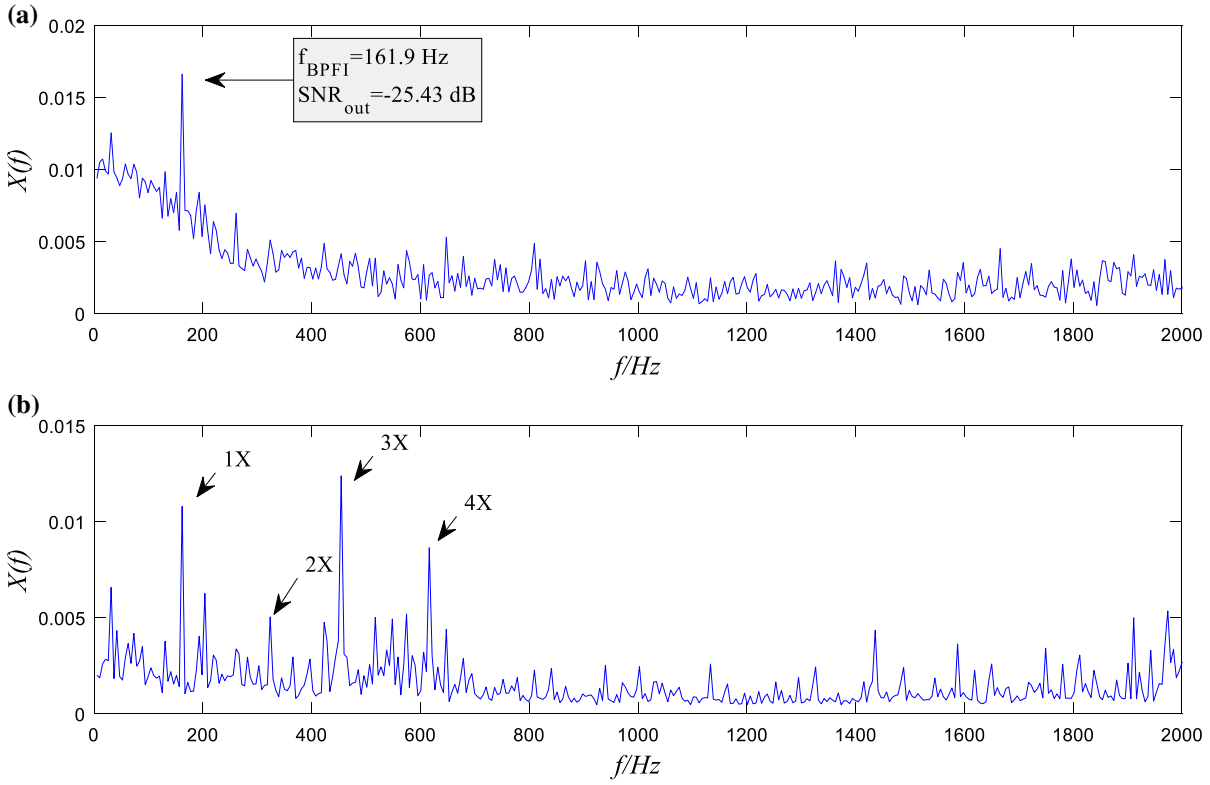

Fig. 13 Detection results with the test signal inputting the MPASR model of the standard tri-stable system. **a** $k = 15$, $m = 2.8$, $p = 0.5$ and $q = 1.2$; **b** $k = 15$, $m = 1.1$, $p = 0.6$ and $q = 1.2$

model of the standard tri-stable system, a weak-signal detection method is proposed for incipient fault diagnosis. At last, the proposed method is employed to diagnose the shaft-bending fault in a sliding-bearing system and the rolling bearing inner raceway fault based on the data from CWRU, thus demonstrating the availability and reliability of the proposed approach.

Acknowledgements This work was supported by Natural Science Foundation of Jiangxi Province (CN) (Grant No. 20161BAB216111), Postdoctoral Innovative Talents Support Program of China (No. BX20180250), Science and Technology Research Project of Education Department of Jiangxi Province (Grant No. GJJ150068) and Key Laboratory of Lightweight and High Strength Structural Materials of Jiangxi Province (Grant No. 20171BCD40003).

Compliance with ethical standards

Conflict of interest The authors declare that they have no conflict of interest.

References

1. Chen, J., Li, Z., Pan, J., Chen, G., Zi, Y., Yuan, J., Chen, B., He, Z.: Wavelet transform based on inner product in fault diagnosis of rotating machinery: a review. Mech. Syst. Signal Process. **70–71**, 1–35 (2016)
2. Shi, H., Li, W.: The application of chaotic oscillator in detecting weak resonant signal of mems resonator. Rev. Sci. Instrum. **88**(5), 055003 (2017)
3. Feng, Z., Zhang, D., Zuo, M.J.: Adaptive mode decomposition methods and their applications in signal analysis for machinery fault diagnosis: a review with examples. IEEE Access **5**, 24301–24331 (2017)
4. Benzi, R., Sutera, A., Vulpiani, A.: The mechanism of stochastic resonance. J. Phys. Math. General **14**(11), L453–L457 (1981)
5. Fauve, S., Heslot, F.: Stochastic resonance in a bistable system. Phys. Lett. A **97**(1–2), 5–7 (1983)
6. Mcnamara, B., Wiesenfeld, K., Roy, R.: Observation of stochastic resonance in a ring laser. Phys. Rev. Lett. **60**(25), 2626–2629 (1988)
7. He, M., Xu, W., Sun, Z.: Dynamical complexity and stochastic resonance in a bistable system with time delay. Nonlinear Dyn. **79**(3), 1787–1795 (2015)

8. Zhong, S., Zhang, L., Wang, H., Ma, H., Luo, M.: Nonlinear effect of time delay on the generalized stochastic resonance in a fractional oscillator with multiplicative polynomial noise. Nonlinear Dyn. **89**(2), 1327–1340 (2017)
9. Gao, Y., Leng, Y., Javey, A., Tan, D., Liu, J., Fan, S., Lai, Z.: Theoretical and applied research on bistable dual-piezoelectric-cantilever vibration energy harvesting toward realistic ambience. Smart Mater. Struct. **25**(11), 115032 (2016)
10. Zheng, R., Nakano, K., Hu, H., Su, D., Cartmell, M.P.: An application of stochastic resonance for energy harvesting in a bistable vibrating system. J. Sound Vib. **333**(12), 2568–2587 (2014)
11. Kim, H., Tai, W.C., Zhou, S., Zuo, L.: Stochastic resonance energy harvesting for a rotating shaft subject to random and periodic vibrations: influence of potential function asymmetry and frequency sweep. Smart Mater. Struct. **26**(11), 115011 (2017)
12. Lu, S., He, Q., Wang, J.: A review of stochastic resonance in rotating machine fault detection. Mech. Syst. Signal Process. **116**, 230–260 (2019)
13. Lei, Y., Qiao, Z., Xu, X., Lin, J., Niu, S.: An underdamped stochastic resonance method with stable-state matching for incipient fault diagnosis of rolling element bearings. Mech. Syst. Signal Process. **94**, 148–164 (2017)
14. Leng, Y.G., Wang, T.Y., Guo, Y., Xu, Y.G., Fan, S.B.: Engineering signal processing based on bistable stochastic resonance. Mech. Syst. Signal Process. **21**(1), 138–150 (2007)
15. Blekhman, I.I., Sorokin, V.S.: On a "deterministic" explanation of the stochastic resonance phenomenon. Nonlinear Dyn. **93**(2), 767–778 (2018)
16. Xu, Y., Wu, J., Zhang, H.Q., Ma, S.J.: Stochastic resonance phenomenon in an underdamped bistable system driven by weak asymmetric dichotomous noise. Nonlinear Dyn. **70**(1), 531–539 (2012)
17. Zhou, P., Lu, S., Liu, F., Liu, Y., Li, G., Zhao, J.: Novel synthetic index-based adaptive stochastic resonance method and its application in bearing fault diagnosis. J. Sound Vib. **391**, 194–210 (2017)
18. Lai, Z.H., Leng, Y.G.: Generalized parameter-adjusted stochastic resonance of duffing oscillator and its application to weak-signal detection. Sensors **15**(9), 21327–21349 (2015)
19. Agudov, N.V., Krichigin, A.V., Valenti, D., Spagnolo, B.: Stochastic resonance in a trapping overdamped monostable system. Phys. Rev. E **81**(5), 051123 (2010)
20. Yao, M., Xu, W., Ning, L.: Stochastic resonance in a bias monostable system driven by a periodic rectangular signal and uncorrelated noises. Nonlinear Dyn. **67**(1), 329–333 (2012)
21. Qiao, Z., Lei, Y., Lin, J., Jia, F.: An adaptive unsaturated bistable stochastic resonance method and its application in mechanical fault diagnosis. Mech. Syst. Signal Process. **84**, 731–746 (2017)
22. Qin, Y., Tao, Y., He, Y., Tang, B.: Adaptive bistable stochastic resonance and its application in mechanical fault feature extraction. J. Sound Vib. **333**(26), 7386–7400 (2014)
23. Han, D., Li, P., An, S., Shi, P.: Multi-frequency weak signal detection based on wavelet transform and parameter compensation band-pass multi-stable stochastic resonance. Mech. Syst. Signal Process. **70–71**, 995–1010 (2016)
24. Li, J., Chen, X., He, Z.: Multi-stable stochastic resonance and its application research on mechanical fault diagnosis. J. Sound Vib. **332**(22), 5999–6015 (2013)
25. Arathi, S., Rajasekar, S.: Impact of the depth of the wells and multifractal analysis on stochastic resonance in a triple-well system. Phys. Scr. **84**(6), 065011 (2011)
26. Zhang, H., Xu, Y., Xu, W., Li, X.: Logical stochastic resonance in triple-well potential systems driven by colored noise. Chaos **22**(4), 043130 (2012)
27. Zhang, H., Yang, T., Xu, W., Xu, Y.: Effects of non-gaussian noise on logical stochastic resonance in a triple-well potential system. Nonlinear Dyn. **76**(1), 649–656 (2014)
28. Shi, P., Li, P., An, S., Han, D.: Stochastic resonance in a multistable system driven by gaussian noise. Discrete Dyn. Nat. Soc. **2016**, 1093562 (2016). https://doi.org/10.1155/2016/1093562
29. Shi, P., Su, X., Han, D., Fu, R., Ma, X.: The stable state properties and mean first-passage time of tristable system driven by non-correlated additive and multiplicative non-gaussian noise. Chin. J. Phys. **55**(5), 2124–2133 (2017)
30. Shi, P., An, S., Li, P., Han, D.: Signal feature extraction based on cascaded multi-stable stochastic resonance denoising and emd method. Measurement **90**, 318–328 (2016)
31. Lu, S., He, Q., Zhang, H., Zhang, S., Kong, F.: Note: signal amplification and filtering with a tristable stochastic resonance cantilever. Rev. Sci. Instrum. **84**(2), 026110 (2013)
32. Lu, S., He, Q., Dai, D., Kong, F.: Periodic fault signal enhancement in rotating machine vibrations via stochastic resonance. J. Vib. Control **22**(20), 4227–4246 (2016)
33. Lai, Z.H., Leng, Y.G.: Dynamic response and stochastic resonance of a tri-stable system. Acta Phys. Sin. **64**(20), 200503 (2015)
34. Ghosh, P.K., Bag, B.C., Ray, D.S.: Interference of stochastic resonances: splitting of kramers' rate. Phys. Rev. E Stat. Nonlinear Soft Matter Phys. **75**(3 Pt 1), 032101 (2007)
35. Lu, J., Huang, M., Yang, J.-J.: A novel spectrum sensing method based on tri-stable stochastic resonance and quantum particle swarm optimization. Wirel. Pers. Commun. **95**(3), 2635–2647 (2017)
36. Lai, Z.H., Leng, Y.G.: Weak-signal detection based on the stochastic resonance of bistable duffing oscillator and its application in incipient fault diagnosis. Mech. Syst. Signal Process. **81**, 60–74 (2016)
37. Smith, W.A., Randall, R.B.: Rolling element bearing diagnostics using the case western reserve university data: a benchmark study. Mech. Syst. Signal Process. **64–65**, 100–131 (2015)